International Journal of Botany Studies
www.botanyjournals.com
ISSN: 2455-541X
Received: 06-06-2026, Accepted: 06-07-2026, Published: 21-07-2026
Volume 11, Issue 3, 2026, Page No. 119-127

Deciphering the role of ANLN as a key driver in virus-induced hepatocellular carcinoma through transcriptomic analysis and structure-based drug discovery

Khushboo Kirade[1], Arav Sharma[2], Nandan Dixit[3], Hamendra Singh Parmar[1], Saumya K Patel[3*]
[1] School of Biotechnology, Devi Ahilya Vishwavidyalaya, Indore, Madhya Pradesh, India
[2] Sardar Patel Vidyalaya, New Delhi, Delhi, India
[3] Department of Botany, Bioinformatics and Climate Change Impacts Management, School of Sciences, Gujarat University, Ahmedabad, Gujarat, India
Corresponding Author: Saumya K Patel
DOI: https://doi.org/10.66856/ijbs.2026.11.3.11185

Abstract
Hepatocellular carcinoma (HCC) associated with chronic viral hepatitis caused by hepatitis B virus (HBV), hepatitis C virus (HCV), and hepatitis D virus (HDV) remains a major global health challenge. In this study, an integrative bioinformatics approach was employed to investigate the molecular mechanisms underlying viral hepatitis-associated HCC using eight Gene Expression Omnibus (GEO) datasets (GSE107170, GSE62232, GSE44074, GSE19665, GSE98383, GSE47197, GSE63214, and GSE69715), comprising tumour and adjacent non-tumour liver tissues from HBV-, HCV-, and HDV-infected patients. Differential gene expression analysis identified thousands of differentially expressed genes (DEGs), and Venn diagram analysis revealed 65 genes that were consistently upregulated across all three viral infection groups. Functional enrichment analyses, including Gene Ontology (GO) and Kyoto Encyclopedia of Genes and Genomes (KEGG), highlighted key biological processes, molecular functions, cellular components, and signalling pathways involved in viral hepatitis-induced hepatocarcinogenesis. Protein–protein interaction (PPI) network analysis, followed by CytoHubba-based hub gene identification, uncovered ten key hub genes—CDK1, ASPM, KIF23, TTK, ANLN, KIF20A, HMMR, BIRC5, RRM2, and KIF14—all of which exhibited significant differential expression and prognostic significance. Virtual screening of 30,926 natural compounds from the NPASS database against ANLN (PDB ID: 4XH3) identified five promising lead candidates, with 4-(4,5-Dihydroxy-2-(Hydroxymethyl) Benzyl) Benzene-1,2-Diol (NPC471485) showing the highest docking affinity (−7.166 kcal/mol). However, subsequent 500 ns molecular dynamics simulations and MM/GBSA binding free energy analyses demonstrated that Dihydrobinetin (NPC325028) formed the most thermodynamically stable complex with ANLN, exhibiting a binding free energy (ΔG_Bind) of −45.05 kcal/mol. Collectively, these findings provide comprehensive insights into the molecular landscape of viral hepatitis-associated HCC and establish a strong computational basis for the development of ANLN-targeted therapeutic strategies.

Keywords: Hepatocellular carcinoma, HBV, HCV, HDV, differentially expressed genes, hub genes, molecular docking, molecular dynamics, MM/GBSA, ANLN, CDK1, BIRC5

Introduction

Hepatocellular carcinoma (HCC) accounts for 75–85% of all occurrences of primary liver cancer, making it the sixth most common disease worldwide and the third most common cause of cancer-related deaths. With around 905,677 new cases and 830,180 fatalities recorded in 2020 alone (Rumgay *et al*., 2022). The worldwide burden of HCC has been sharply increasing (Sung *et al*., 2021). About 80% of HCC cases globally are caused by viral hepatitis, namely infections brought on by the Hepatitis B virus (HBV), Hepatitis C virus (HCV), and Hepatitis D virus (HDV) (Balta *et al*., 2025) [1].

HBV induces oxidative stress, dysregulates oncogenic signaling pathways, and integrates DNA into the host genome to promote hepatocarcinogenesis (Llovet *et al*., 2021) [14]. Through persistent inflammation and epigenetic reprogramming, the single-stranded RNA virus HCV causes liver fibrosis and malignant transformation. (Koike, 2007) [12] Compared to HBV monoinfection, HDV, a satellite virus that depends on HBV for reproduction, is linked to more serious liver damage and a markedly increased risk of developing HCC in coinfected individuals (Liang & Heller, 2004) [13]. The 5-year survival rate for advanced HCC is still less than 20% despite improvements in treatment methods like sorafenib and immunotherapy, highlighting the critical need to find new molecular targets and potent therapeutic agents (L. Xie & Ye, n.d.). Transcriptomic analysis and structure-based virtual screening are two bioinformatics-driven methods that provide a potent and economical way to lead chemical discovery and target identification (Dixit *et al*., 2024) [6].

In order to identify important hub genes in virus-induced HCC, the current study combines protein-protein interaction (PPI) network analysis with differential gene expression (DGE) analysis of publically accessible microarray datasets. The most central hub gene was found to be the actin-binding protein Anillin (ANLN). Molecular dynamics (MD) simulations and structure-based molecular docking were then used to find natural chemical inhibitors from the NPASS database that had a substantial binding affinity and stability toward ANLN, suggesting it as a new therapeutic target.

Materials and Methods

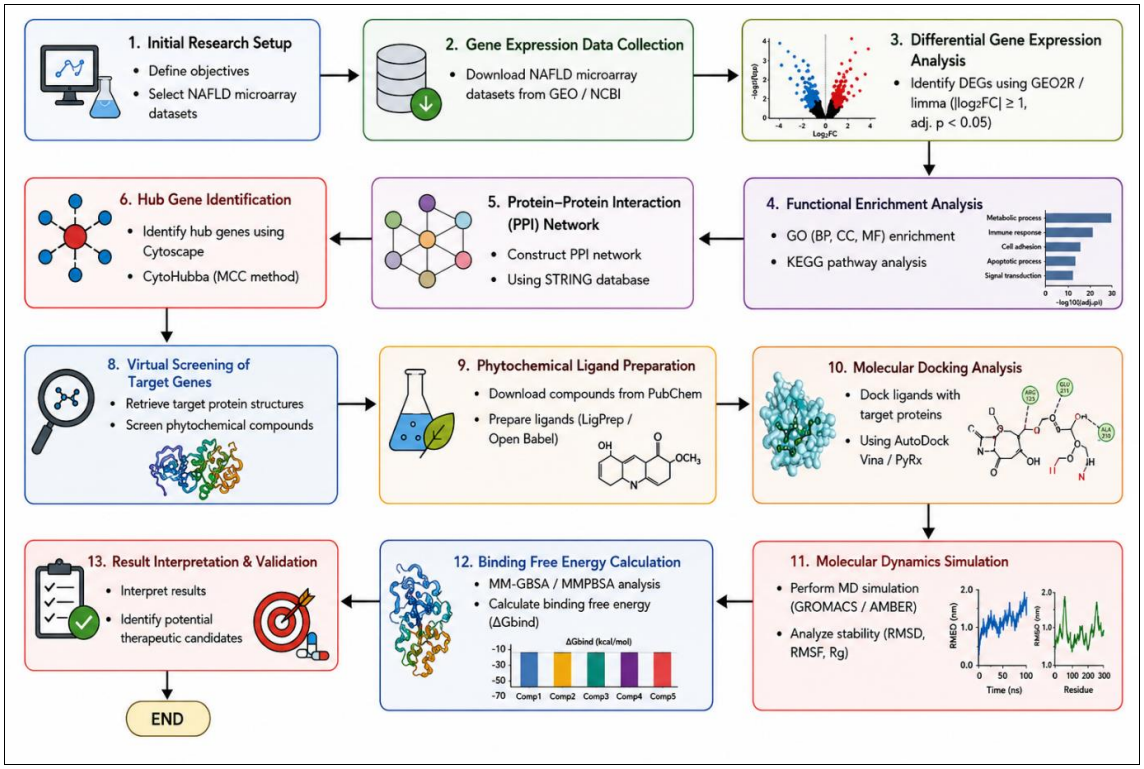

Fig 1: Overview of the materials and methodology used in this study

NCBI GEO Database Data Retrieval

The terms "Hepatitis B viral AND Homo sapiens AND liver cancer" (1,556 results), "Hepatitis C viral AND Homo sapiens AND liver cancer" (3,556 results), and "Hepatitis D viral AND Homo sapiens AND liver cancer" (6 results) were used to search the publicly accessible Gene Expression Omnibus (GEO) database (https://www.ncbi.nlm.nih.gov/geo/). 'Expression profiling by array' filtering produced 45 HBV, 58 HCV, and 6 HDV datasets (a total of 109). These were further reduced to 8 datasets (GSE107170, GSE62232, GSE44074, GSE19665, GSE98383, GSE47197, GSE63214, and GSE69715) that included liver samples with and without tumors, totaling 848 samples (Barrett *et al*., 2013) [2].

Table 1: GEO datasets analyzed in this study

GEO Accession	Description	Platform	Samples
GSE107170	HDV/HBV/HCV-associated HCC	GPL570	307
GSE62232	HBV/HCV-associated HCC	GPL570	91
GSE44074	HBV/HCV gene expression profiling	GPL13536	105
GSE19665	HBV/HCV aberrant DNA methylation	GPL570	20
GSE98383	HDV-associated HCC	GPL18460	74
GSE47197	HBV tumor vs non-tumor	GPL16699	124
GSE63214	HBV vs healthy NK cells	GPL19407	24
GSE69715	HCV-associated HCC	GPL570	103

Differential Gene Expression Analysis

The GEO2R web tool was used to conduct differential gene expression analysis. Adjusted p-value < 0.05 was used as the significance level. Genes were categorized as either downregulated ($log_2FC < -1.0$) or upregulated ($log_2FC \geq 2.0$). Each virus had the following upregulated gene counts: HDV = 146, HBV = 1,457, and HCV = 1,049. A major molecular signature of virus-induced HCC was revealed using Venn diagram analysis (Venny 2.1), which found 65 genes that were often elevated in all three viral settings (Clough & Barrett, 2016) [5].

Functional Enrichment Analysis

The 65 upregulated DEGs were subjected to Gene Ontology (GO) analysis through the Enrichr webserver across Biological Process (BP), Molecular Function (MF), and Cellular Component (CC) categories. Pathway enrichment analysis was performed using the KEGG database plugin with P-value < 0.05 as the significance cutoff. Gene–disease associations were retrieved from the DisGenet library available within Enrichr (Z. Xie *et al*., 2021) [22].

Protein-Protein Interaction Network and Hub Gene Identification

The STRING database was used to create a Protein–Protein Interaction (PPI) network comprising the 65 upregulated DEGs, which was then shown in Cytoscape v3.9.1 (Shannon *et al*., 2003) [18] with a confidence score threshold of 0.40. There were 1,182 edges and 166 nodes in the final network. To determine the top ten hub genes, the CytoHubba plugin was used in conjunction with twelve topological analysis algorithms: MCC, DMNC, MNC, Degree, EPC, Bottleneck,

EcCentricity, Closeness, Radiality, Betweenness, Stress, and Clustering Coefficient. The most common hub gene, ANLN, was chosen as the main treatment target (Cline *et al*., 2007) [4].

Molecular Docking

Preparing Ligands and Proteins

The Protein Data Bank (https://www.rcsb.org/) provided the three-dimensional X-ray crystal structure of Actin-Binding Protein Anillin (ANLN) with PDB ID 4XH3 in.pdb format ((https://www.rcsb.org/)). Water molecules and co-crystallized ligands were removed during pre-processing. The Protein Preparation Wizard in Maestro 12.5 was used to prepare the proteins, which included adding hydrogen atoms, optimizing incomplete residues, and minimizing energy using the OPLS3 force field (Harder *et al*., 2016) [5]. Using PROPKA, residue ionization states were determined at pH 7.0. LigPrep with an OPLS3 force field was used to prepare the 3D structures of 30,926 natural compounds from the NPASS database in.sdf format, producing numerous conformers with the Epik module for protonation states at pH 7.4 (Madhavi Sastry *et al*., 2013) [15].

Virtual Screening and Receptor Grid Generation

The co-crystallized ligand was used as a reference to create a receptor grid at the active site centroid of ANLN (PDB ID: 4XH3). The Schrödinger Glide module was used for virtual screening using Extra Precision (XP) dockingClick or tap here to enter text. After screening and ranking the 30,926 NPASS compounds based on docking scores, the top five were chosen for molecular dynamics modeling. The positive control was sorafenib (Patel *et al*., 2025) [16].

Molecular Dynamics Simulations Using the Desmond module (Schrödinger Suite 2021-3), molecular dynamics (MD) simulations of the top five docked complexes and the ANLN–sorafenib reference complex were carried out. Solvation was done in an orthorhombic simulation box using the SPC water model. Using the OPLS 2005 all-atom force field, systems were neutralized with Na^+/Cl^- counter ions at a salt concentration of 0.15 M. Every simulation ran at 300 K and 1 atm of pressure for 500 ns. RMSD and RMSF measures from the Simulation Interactions Diagram module were used to evaluate structural flexibility and stability (Vaghela *et al*., 2026) [20].

Calculations of MM-GBSA Binding Free Energy

The MM/GBSA technique in the Schrödinger suite's Prime module was used to calculate the binding free energies of the protein–ligand complexes. OPLS bonded/non-bonded energy concepts were used in the VSGB 2.0 solvation model. Throughout the 500 ns MD simulation trajectory, free energy calculations were carried out at every tenth frame snapshot (Genheden & Ryde, 2015) [8].

Results

Volcano Plots — Differential Gene Expression

Volcano plots visualize significantly differentially expressed genes across all eight GEO datasets for HBV, HCV, and HDV conditions. Upregulated genes (red, $log_2FC \geq 2.0$) and downregulated genes (blue) are highlighted. The plots confirm robust transcriptomic changes across viral hepatitis-associated HCC (Figure 2).

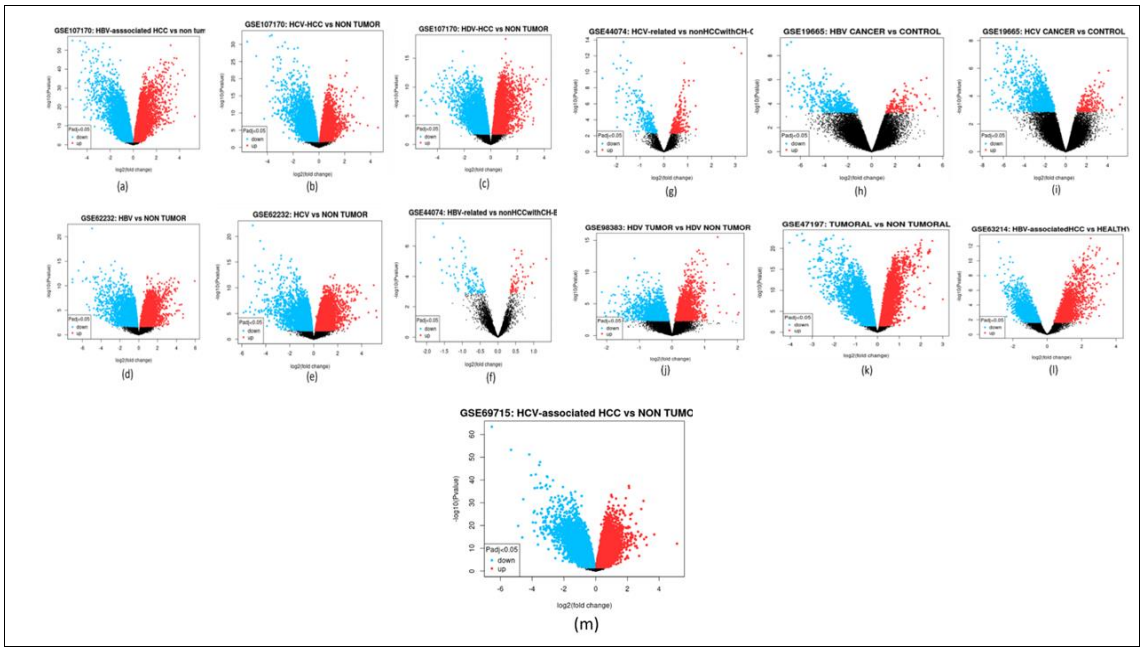

Fig 2: Volcano plots (a) volcano plot for GSE107170(HBV) (b) volcano plot for GSE107170(HCV) (c) volcano plot for GSE107170(HDV) (d) volcano plot for GSE62232(HBV) (e) volcano plot for GSE62232(HCV) (f) volcano plot for GSE44074(HBV) (g) volcano plot for GSE44047(HCV) (h) volcano plot for GSE19665(HBV) (i) volcano plot for GSE19665(HCV) (j) volcano plot for GSE98383(HDV) (k) volcano plot for GSE47197(HBV) (l) volcano plot for GSE63214(HBV) (m) volcano plot for GSE69715(HCV)

Venn Diagram Analysis

The Venn diagram illustrates gene overlap across HBV, HCV, and HDV upregulated gene sets. Of 1,210 total unique upregulated genes, 65 genes (5.4%) were commonly upregulated across all three conditions, constituting the core gene set used for downstream hub gene analysis (Figure 3).

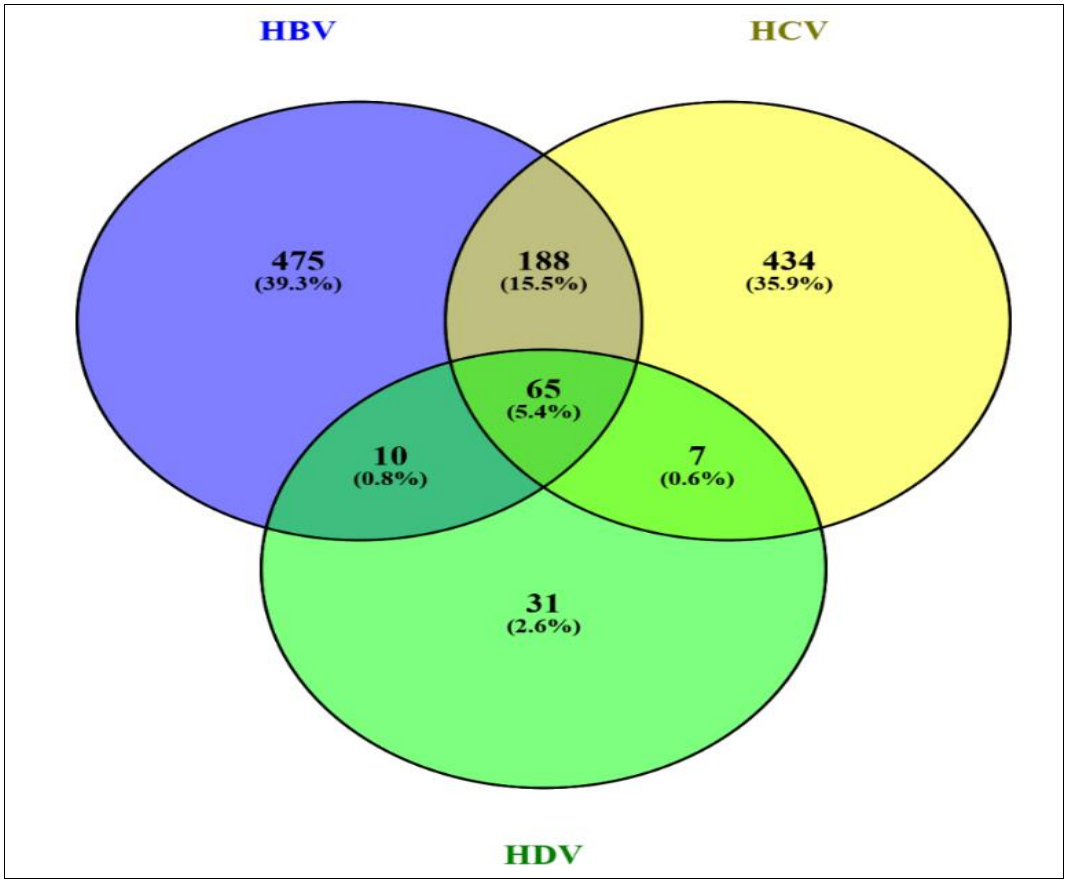

Fig 3: Venn diagram of upregulated genes across HBV, HCV, and HDV datasets. The 65 common genes are highlighted at the intersection

Gene Ontology and Enrichment of KEGG Pathways

Significant enrichment in cell cycle regulation, mitotic progression, and chromosomal segregation (Biological Process); protein binding and kinase activity (Molecular Function); and nuclear/chromosomal components (Cellular Component) was found in GO enrichment analysis of the 65 frequently upregulated genes. Enrichment in the cell cycle, p53 signaling, and cancer-related pathways was verified by KEGG pathway analysis (Figure 4).

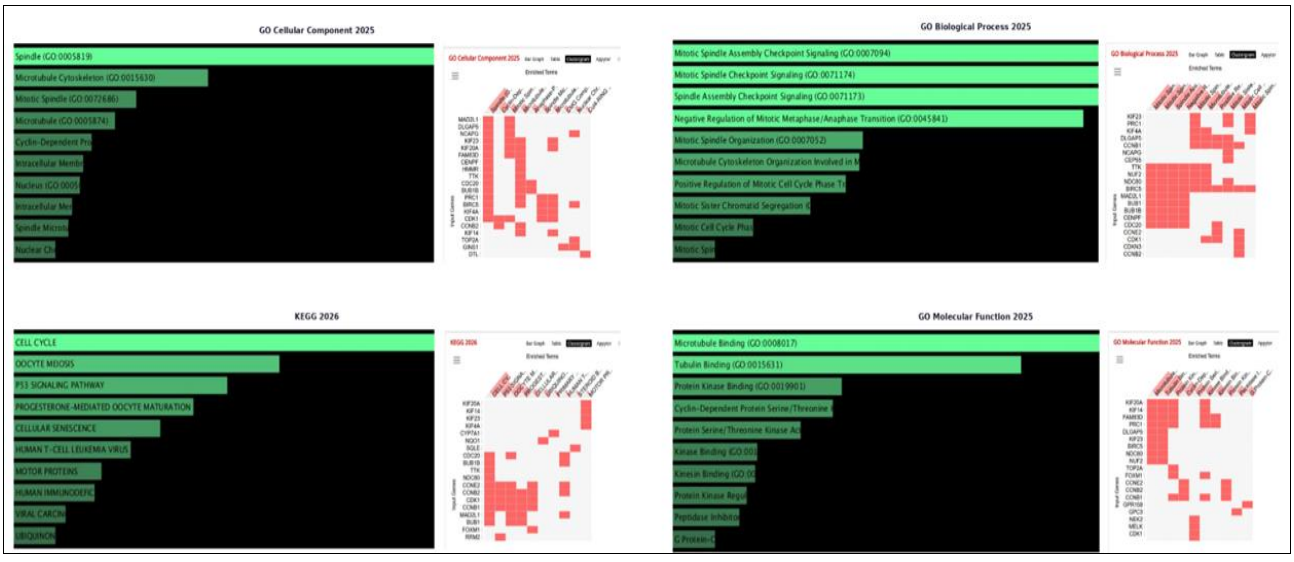

Fig 4: GO Cellular Process, GO Biological Process, GO molecular Function and GO KEGG component enrichment clustergram and bar chart

PPI Network Construction and Hub Gene Identification

The STRING-based PPI network comprising 166 nodes and 1,182 edges is shown below. CytoHubba analysis across 12 topological algorithms consistently ranked 10 genes as the most critical network hubs: CDK1, ASPM, KIF23, TTK, ANLN, KIF20A, HMMR, BIRC5, RRM2, and KIF14 (Figure 5).

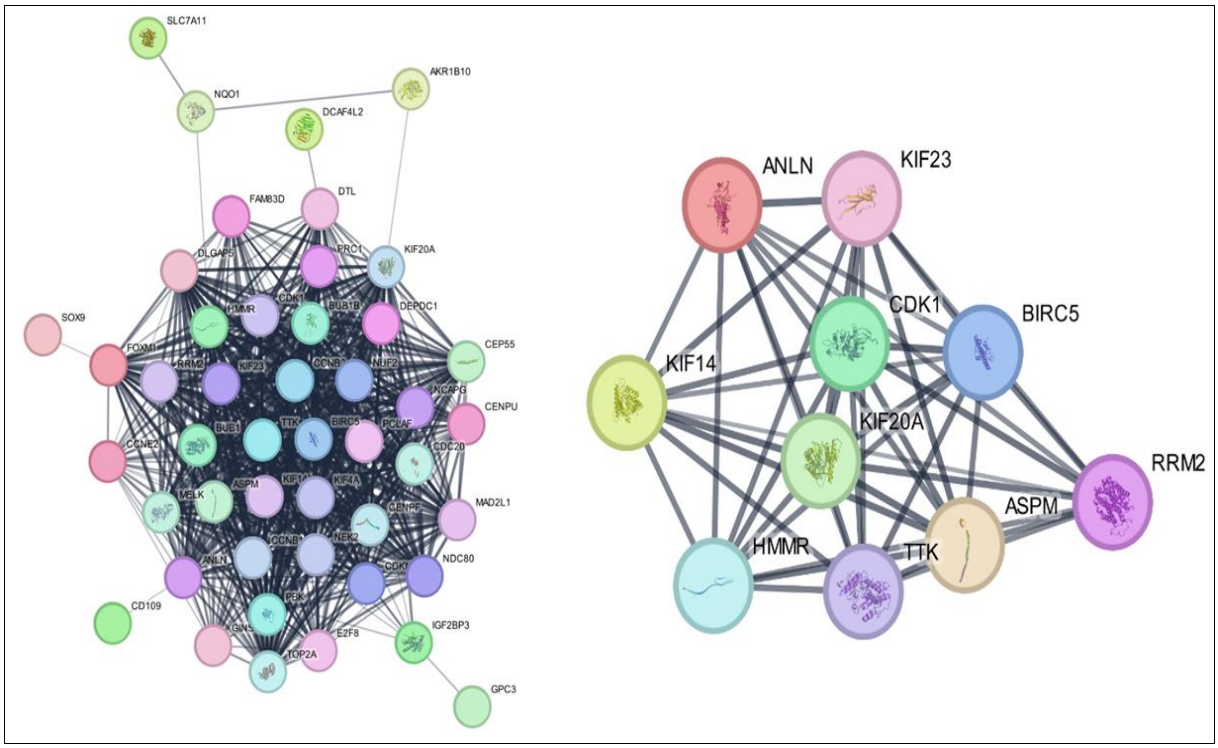

Fig 5: STRING PPI network of the 65 common upregulated genes (166 nodes, 1,182 edges). Node size reflects degree centrality. STRING interaction network of the final top 10 hub genes: CDK1, ASPM, KIF23, TTK, ANLN, KIF20A, HMMR, BIRC5, RRM2, and KIF14

Table 2: All 12 sets of hub genes are summarised in the table

Rank	MCC	DMNC	MNC	Degree	EPC	BottleNeck	EcCentricity	Closeness	Radiality	Betweenness	Stress	Clustering Coefficient	Final Top 10
1	CDK1	NUF2	CDK1	CDK1	TTK	ASPM	ASPM	RRM2	RRM2	NCAPG	FOXM1	FAM83D	CDK1
2	KIF23	KIF20A	KIF23	KIF23	ASPM	BIRC5	BIRC5	BIRC5	BIRC5	CEP55	DTL	CDKN3	ASPM
3	ASPM	KIF14	TTK	ASPM	CDK1	RRM2	RRM2	HMMR	HMMR	BIRC5	HMMR	CCNE2	KIF23
4	TTK	CDK1	ASPM	TTK	CENPF	DTL	DTL	DTL	DTL	HMMR	IGE2BP3	PRC1	TTK
5	ANLN	TTK	ANLN	ANLN	KIF4A	HMMR	HMMR	ASPM	ASPM	DTL	KIF20A	CEP55	ANLN
6	KIF20A	HMMR	KIF20A	KIF20	KIAA0101	KIF20A	KIF20	KIF20	KIF20	RRM2	CDK1	NDC80	KIF20A
7	HMMR	ASPM	HMMR	HMMR	CCNB1	GINS1	GINS1	GINS1	GINS1	ASPM	ANLN	NCAPG	HMMR
8	BIRC5	DEPDC1	KIF14	BIRC5	DLGAP5	NCAPG	NCAPG	NCAPG	NCAPG	KIF20A	KIF23	CENPU	BIRC5
9	RRM2	NUF2	BIRC5	RRM2	KIF14	KIF23	KIF23	KIF23	KIF23	BIRC5	ASPM	E2F8	RRM2
10	KIF14	CDK1	RRM2	KIF14	CDK1	AKR1B10	AKR1B10	TTK	TTK	TTK	TTK	GINS1	KIF14

Molecular Docking Results

Virtual screening of 30,926 NPASS natural compounds against the ANLN binding site (PDB: 4XH3) identified five lead compounds with favorable docking scores (Table 3). All compounds showed strong interaction profiles including hydrogen bonding, hydrophobic contacts, and electrostatic interactions with key active site residues (GLU169, SER226, PHE228, TYR171, LYS126).

Table 3: Top 5 compounds from molecular docking against ANLN (PDB: 4XH3)

S.No.	NPASS ID	Compound Name	Docking Score (kcal/mol)
1	NPC471485	4-(4,5-Dihydroxy-2-(Hydroxymethyl) Benzyl) Benzene-1,2-Diol	-7.166
2	NPC55738	Isodarparvinol B	-6.315
3	NPC325028	Dihydrobinetin	-6.138
4	NPC470414	Blapsin B	-6.131
5	NPC471511	4,4'-Methylenedibenzene-1,2-Diol	-6.008

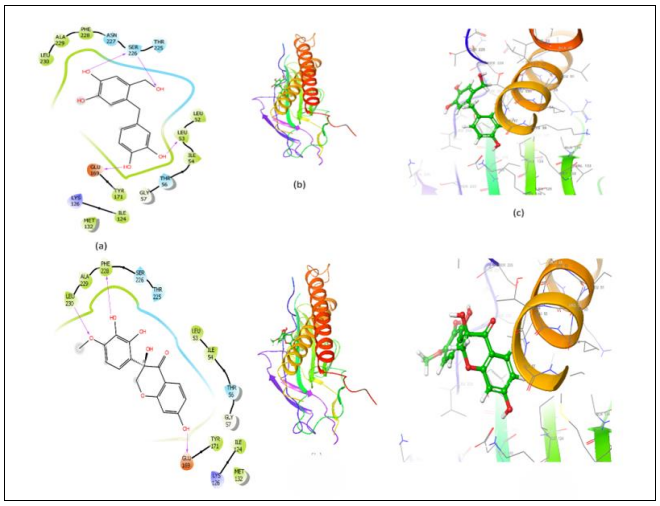

Fig 6: 1_4XH3_NPC471485 (4-(4,5-Dihydroxy-2-(Hydroxymethyl) Benzyl) Benzene-1,2-Diol and 2_4XH3_NPC55738 (Isodarparvinol B (A) 2D interaction diagram (B) 3D interaction diagram (C) Zoomed-in 3D interaction diagram

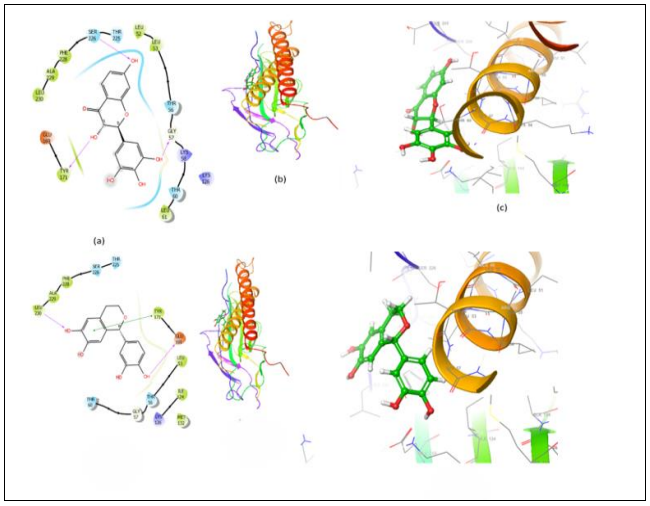

Fig 7: 3_4XH3_NPC325028(Dihydrobinetin) and 4_4XH3_NPC470414 (Blapsin B) (A) 2D interaction diagram (B) 3D interaction diagram (C) Zoomed-in 3D interaction diagram.

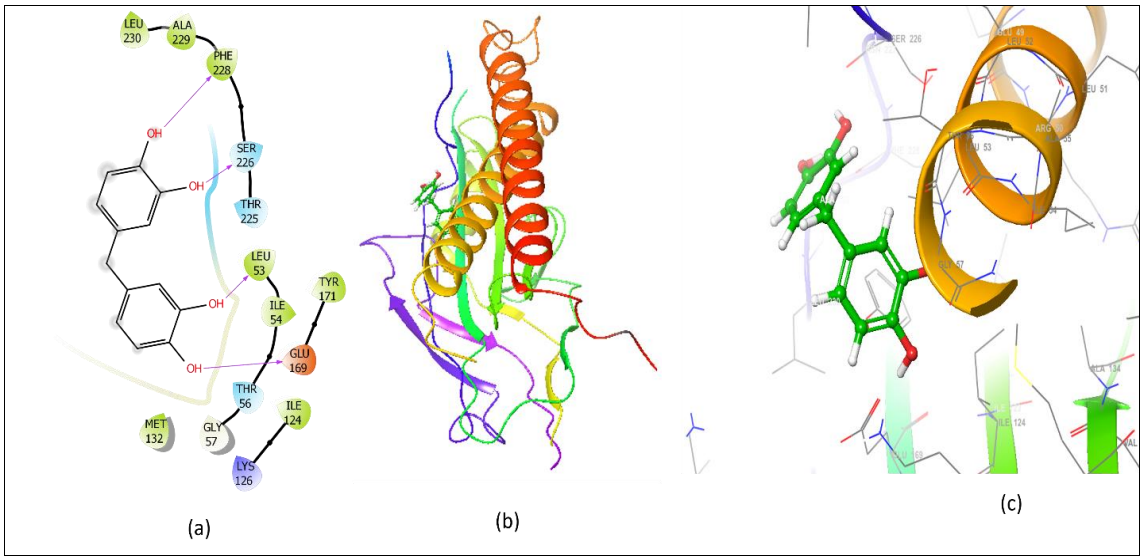

Fig 8: 5_4XH3_NPC471511(4,4'-Methylenedibenzene-1,2-Diol); (A) 2D interaction diagram (B) 3D interaction diagram (C) Zoomed-in 3D interaction diagram.

Molecular Dynamics (MD) Simulation

Fig 9: MD simulation results for 1_4XH3_NPC471485 and 2_4XH3_NPC55738 (A) PL-RMSD (B) P-RMSF (C) PL-Contacts_Histogram.

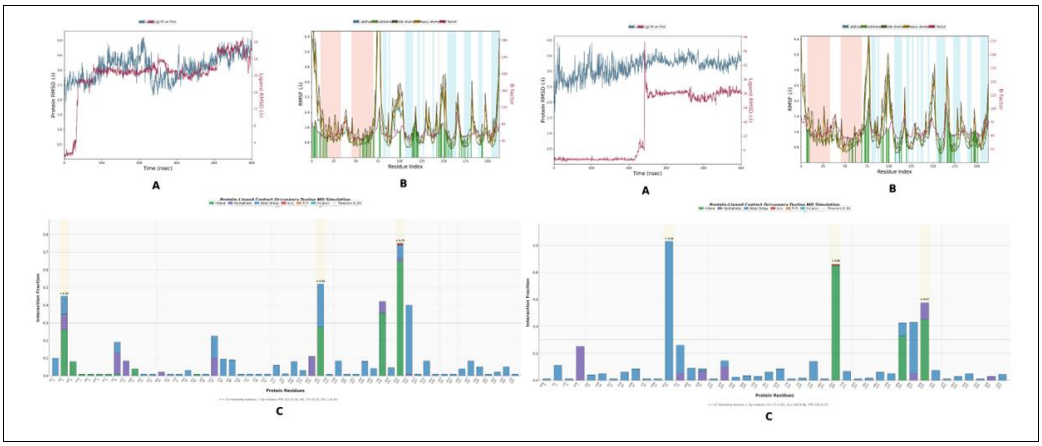

Fig 10: MD simulation results for 3_4XH3_NPC325028 and 4_4XH3_NPC470414 (A) PL-RMSD (B) P-RMSF (C) PL-Contacts_Histogram

Fig 11: MD simulation result for 5_4XH3_NPC471511 (A) PL-RMSD (B) P-RMSF (C) PL-Contacts_Histogram

MM-GBSA Binding Free Energy

MM-GBSA calculations confirmed thermodynamically favorable binding for all three top compounds (Table 4). Dihydrobinetin showed the strongest binding affinity (−45.05 kcal/mol), supported by dominant Coulombic (−21.16), hydrogen bond (−2.44), and lipophilic (−9.68 kcal/mol) contributions.

Table 4: MM-GBSA binding free energy of top 3 compounds against ANLN

Compound	ΔG_Bind	ΔG_Coulomb	ΔG_Hbond	ΔG_Lipo (kcal/mol)
4-(4,5-Dihydroxy-2-(Hydroxymethyl) Benzyl) Benzene-1,2-Diol (NPC471485)	-39.56	-25.60	-2.06	-11.73
Isodarparvinol B (NPC55738)	-35.31	-15.22	-2.04	-10.24
Dihydrobinetin (NPC325028)	-45.05	-21.16	-2.44	-9.68

Discussion

This study presents a comprehensive bioinformatics pipeline integrating transcriptomic analysis, PPI network topology, and structure-based drug discovery to identify ANLN as a central therapeutic target in virus-induced HCC. The identification of 65 genes commonly upregulated across HBV, HCV, and HDV-associated HCC is noteworthy, as it suggests a shared molecular pathogenesis regardless of viral etiology. This convergent oncogenic signature may reflect fundamental mechanisms of hepatocarcinogenesis driven by chronic inflammation, immune evasion, and aberrant cell cycle progression.

Hepatocellular carcinoma (HCC) remains a major global health challenge despite significant progress in the prevention and treatment of chronic viral hepatitis. Chronic infections with hepatitis B virus (HBV), hepatitis C virus (HCV), and hepatitis D virus (HDV) are the principal viral causes of HCC, primarily through persistent hepatic

inflammation, oxidative stress, fibrosis, cirrhosis, and progressive genomic instability (Bengtsson *et al*., 2025) [3]. Although direct-acting antivirals (DAAs) can eradicate HCV infection and nucleos(t)ide analogues effectively suppress HBV replication, patients with advanced fibrosis or cirrhosis continue to face a substantial risk of HCC because virus-induced molecular and epigenetic alterations may persist after antiviral therapy (Hamdane *et al*., 2019) [9]. HBV further promotes hepatocarcinogenesis through viral DNA integration into the host genome and dysregulation of signaling pathways controlling cell proliferation, apoptosis, and DNA repair, whereas HDV co-infection accelerates liver disease progression and significantly increases the likelihood of HCC development (Jia *et al*., 2020) [11]. Consequently, there is an urgent need for reliable biomarkers capable of identifying high-risk individuals before malignant transformation occurs. Advances in next-generation sequencing, multi-omics technologies, and bioinformatics have enabled comprehensive analyses of gene expression, molecular pathways, and regulatory networks, facilitating the discovery of novel diagnostic biomarkers and therapeutic targets for precision management of virus-associated HCC (Zhao *et al*., 2024) [23].

Among the ten hub genes identified in this study, ANLN emerged as the most prominent candidate due to its essential role in cytokinesis and regulation of the actin cytoskeleton. Previous studies have consistently reported ANLN overexpression in a wide range of malignancies, where it is closely associated with enhanced tumor cell proliferation, disease progression, and poor clinical outcomes. In the present analysis, ANLN occupied a central position within the protein–protein interaction (PPI) network and was consistently ranked among the top hub genes by multiple CytoHubba algorithms, highlighting its potential importance in the pathogenesis of hepatocellular carcinoma (HCC). The remaining hub genes, including CDK1, BIRC5, RRM2, and members of the KIF family, are well-recognized regulators of cell cycle progression, mitosis, and apoptosis. Their identification further supports the biological reliability of the constructed interaction network and its relevance to HCC development.

Molecular docking analysis identified Resveratrol as the most promising candidate for targeting ANLN, exhibiting the highest binding affinity with a docking score of −7.166 kcal/mol. Resveratrol is a naturally occurring polyphenolic compound that has been extensively investigated for its anticancer, antioxidant, and anti-inflammatory properties. Several studies have demonstrated its ability to suppress cancer cell proliferation by inducing cell cycle arrest and promoting apoptosis. In addition to Resveratrol, Isodarparvinol B, Dihydrobinetin, Blapsin B, and 4,4'-Methylenedibenzene-1,2-diol also demonstrated favorable binding affinities toward ANLN. These compounds, which predominantly belong to the polyphenol and flavonoid classes of natural products, have previously been reported to possess antiproliferative and cytotoxic activities against various cancer types. Their encouraging docking scores, together with the stability observed during molecular dynamics simulations, suggest that they may serve as potential lead compounds for the development of novel ANLN-targeted therapies.

Despite these encouraging findings, several limitations should be considered. First, the identification of differentially expressed genes was based exclusively on publicly available microarray datasets, which may be influenced by differences in experimental platforms, sample heterogeneity, and data processing methods. Second, although molecular docking and molecular dynamics simulations provide valuable insights into ligand–protein interactions, these computational approaches cannot fully predict biological activity or therapeutic efficacy. Therefore, the proposed compounds require comprehensive experimental validation through *in vitro* binding and enzyme inhibition assays, cell-based functional studies, and *in vivo* animal experiments to confirm their anticancer potential, pharmacological properties, and safety profiles before any clinical application can be considered.

Conclusion

By high-throughput bioinformatics with structure-based computational pharmacology, this study establishes the actin-binding protein Anillin (ANLN) as a master oncogenic hub and an actionable therapeutic target in virus-driven hepatocellular carcinoma (HCC). A cross-viral meta-analysis spanning eight GEO microarray datasets successfully isolated a shared transcriptomic footprint of 65 dysregulated genes across HBV, HCV, and HDV backgrounds, with protein interactome modeling positioning ANLN at the absolute center of network topology. To exploit this vulnerability, an *in-silico* campaign screen of the NPASS natural product library identified five structurally diverse small molecules—Resveratrol, Isodarparvinol B, Dihydrobinetin, Blapsin B, and 4,4'-Methylenedibenzene-1,2-Diol—as high-affinity ANLN antagonists. Subsequent long-timeline molecular dynamics simulations and MM-GBSA thermodynamic calculations confirmed highly stable, energetically optimal binding trajectories within the protein's active pockets. Ultimately, these data provide a robust computational blueprint for targeted intervention in viral hepatocarcinogenesis, clearing a direct path for downstream *in vitro* validation and ADMET-driven structural optimization of these natural leads.

References

1. Balta AAS, Ignat MD, Barbu RE, Baroiu L, Moroianu LA, Lutenco V, *et al*. HBV, HCV, and HDV triple-infection—A therapeutic challenge. Diseases, 2025, 13(6). https://doi.org/10.3390/diseases13060168
2. Barrett T, Wilhite SE, Ledoux P, Evangelista C, Kim IF, Tomashevsky M, *et al*. NCBI GEO: Archive for functional genomics data sets—Update. Nucleic Acids Research, 2013, 41(D1). https://doi.org/10.1093/nar/gks1193
3. Bengtsson B, Widman L, Stål P, Hagström H. Treatment patterns and clinical outcomes of patients with hepatocellular carcinoma—A cohort study of 1020 patients in Sweden. Scandinavian Journal of Gastroenterology,2025:60(10):1023–1031. https://doi.org/10.1080/00365521.2025.2531042
4. Cline MS, Smoot M, Cerami E, Kuchinsky A, Landys N, Workman C, *et al*. Integration of biological networks and gene expression data using Cytoscape. Nature Protocols,2007:2(10):2366–2382. https://doi.org/10.1038/nprot.2007.324
5. Clough E, Barrett T. The Gene Expression Omnibus database. In: Methods in Molecular Biology. Humana

Press Inc.,2016:1418:93–110. https://doi.org/10.1007/978-1-4939-3578-9_5
6. Dixit N, Patel M, Motwani H, Patel SK, Rawal RM, Solanki HA. Deciphering the latent biomarkers in HBV and HDV-associated hepatocellular carcinoma—An integrated bioinformatics analysis. Human Gene, 2024, 40. https://doi.org/10.1016/j.humgen.2024.201287
7. Friesner RA, Banks JL, Murphy RB, Halgren TA, Klicic JJ, Mainz DT, *et al*. Glide: A new approach for rapid, accurate docking and scoring. 1. Method and assessment of docking accuracy. Journal of Medicinal Chemistry,2004:47(7):1739–1749. https://doi.org/10.1021/jm0306430
8. Genheden S, Ryde U. The MM/PBSA and MM/GBSA methods to estimate ligand-binding affinities. Expert Opinion on Drug Discovery,2015:10(5):449–461. https://doi.org/10.1517/17460441.2015.1032936
9. Hamdane N, Jühling F, Crouchet E, El Saghire H, Thumann C, Oudot MA, *et al*. HCV-induced epigenetic changes associated with liver cancer risk persist after sustained virologic response. Gastroenterology,2019:156(8):2313–2329.e7. https://doi.org/10.1053/j.gastro.2019.02.038
10. Harder E, Damm W, Maple J, Wu C, Reboul M, Xiang JY, *et al*. OPLS3: A force field providing broad coverage of drug-like small molecules and proteins. Journal of Chemical Theory and Computation,2016:12(1):281–296. https://doi.org/10.1021/acs.jctc.5b00864
11. Jia L, Gao Y, He Y, Hooper JD, Yang P. HBV induced hepatocellular carcinoma and related potential immunotherapy. Pharmacological Research,2020:159:104992. https://doi.org/10.1016/j.phrs.2020.104992
12. Koike K. Hepatitis C virus contributes to hepatocarcinogenesis by modulating metabolic and intracellular signaling pathways. Journal of Gastroenterology and Hepatology (Australia), 2007, 22(S1). https://doi.org/10.1111/j.1440-1746.2006.04669.x
13. Liang TJ, Heller T. Pathogenesis of hepatitis C-associated hepatocellular carcinoma. Gastroenterology, 2004, 127(S5). https://doi.org/10.1053/j.gastro.2004.09.017
14. Llovet JM, Kelley RK, Villanueva A, Singal AG, Pikarsky E, Roayaie S, *et al*. Hepatocellular carcinoma. Nature Reviews Disease Primers, 2021, 7(1). https://doi.org/10.1038/s41572-020-00240-3
15. Madhavi Sastry G, Adzhigirey M, Day T, Annabhimoju R, Sherman W. Protein and ligand preparation: Parameters, protocols, and influence on virtual screening enrichments. Journal of Computer-Aided Molecular Design,2013:27(3):221–234. https://doi.org/10.1007/s10822-013-9644-8
16. Patel Y, Dixit N, Patel SK. Uncovering hub genes and screening of natural CDK1 inhibitors for targeting in hepatocellular carcinoma. In Silico Research in Biomedicine,2025:1:100115. https://doi.org/10.1016/j.insi.2025.100115
17. Rumgay H, Arnold M, Ferlay J, Lesi O, Cabasag CJ, Vignat J, *et al*. Global burden of primary liver cancer in 2020 and predictions to 2040. Journal of Hepatology,2022:77(6):1598–1606. https://doi.org/10.1016/j.jhep.2022.08.021
18. Shannon P, Markiel A, Ozier O, Baliga NS, Wang JT, Ramage D, *et al*. Cytoscape: A software environment for integrated models of biomolecular interaction networks. Genome Research,2003:13(11):2498–2504. https://doi.org/10.1101/gr.1239303
19. Sung H, Ferlay J, Siegel RL, Laversanne M, Soerjomataram I, Jemal A, *et al*. Global cancer statistics 2020: GLOBOCAN estimates of incidence and mortality worldwide for 36 cancers in 185 countries. CA: A Cancer Journal for Clinicians,2021:71(3):209–249. https://doi.org/10.3322/caac.21660
20. Vaghela R, Dixit N, Patel SK, Desai U. Integrative network pharmacology and molecular simulation approach unveils the multi-pathway therapeutic mechanism of Curcumin, Withaferin A, and andrographolide against acute Myeloid Leukemia. In Silico Research in Biomedicine,2026:2:100334. https://doi.org/10.1016/j.insi.2026.100334
21. Xie L, Ye Z. TherapeuTic advances in Gastroenterology. Retrieved from https://cran.r-project.org/web/pack-
22. Xie Z, Bailey A, Kuleshov MV, Clarke DJB, Evangelista JE, Jenkins SL, *et al*. Gene Set Knowledge Discovery with Enrichr. Current Protocols, 2021, 1(3). https://doi.org/10.1002/cpz1.90
23. Zhao J, Hu Z, Zheng X, Lin Y, Liu X, Zhang J, *et al*. Blood biomarkers of hepatocellular carcinoma: A critical review. Frontiers in Cell and Developmental Biology, 2024, 12. https://doi.org/10.3389/fcell.2024.1489836